Available online at www.sciencedirect.com

ScienceDirect

IFAC PapersOnline CONFERENCE PAPER ARCHIVE

IFAC PapersOnLine 58-6 (2024) 113–118

Structure-Preserving Discretization of a Polyconvexity-Inspired Formulation for Coupled Nonlinear Electro-Thermo-Elastodynamics

Moritz Hille * **Marlon Franke** * **Felix Zähringer** * **Peter Betsch** *

* *Institute of Mechanics, Karlsruhe Institute of Technology (KIT), Germany (e-mail: Peter.Betsch@kit.edu).*

Abstract: A consistent, structure-preserving space-time discretization for coupled nonlinear electro-thermo-elastodynamical problems is presented. The underlying polyconvexity-inspired mixed framework is facilitated by the properties of the tensor cross product. The elastodynamic problem is then extended by the energy balance as well as Gauss's and Faraday's law to integrate the thermodynamic and electrostatic contribution, respectively. A suitable polyconvexity-inspired internal energy function is chosen to complete the nonlinear, fully coupled electro-thermo-elastodynamical formulation. Additionally, we present a structure-preserving, second-order accurate time integration scheme, utilizing discrete derivatives in the sense of Gonzalez (1996), ensuring a stable and robust simulation even for large time steps. Finally, we assess the numerical performance of our newly developed method through representative examples also showing the possibilities of the framework in the field of boundary control.

Keywords: Nonlinear electro-thermo-elastodynamics, Polyconvexity, Tensor cross product, Structure-preserving discretization

1. INTRODUCTION

Dielectric elastomers (DEs) are classified as smart materials within the group of electroactive polymers, showcasing great potential in the field of control owing to their electrically induced actuation properties. In their basic configuration, DEs comprise an elastomer layer sandwiched between two electrodes. The application of a voltage results in a Coulomb force, leading to a compression of the elastomer layer. DEs can undergo large deformations, with area expansions of up to 1600% (Keplinger et al. (2012)), albeit exhibiting sensitivity to temperature variations (see e.g. Mehnert et al. (2021)). Thus, this paper provides a fully coupled nonlinear thermo-electro-mechanical framework to simulate DEs.

For long-term time-dependent finite element simulations of DEs, employing a stable and robust spatial and temporal discretization is crucial. Energy-momentum (EM) time integration schemes offer superior stability and robustness compared to other classical time integration methods (Simo and Tarnow (1992)). This superiority arises from their inherent ability to preserve the conservation of the total energy, total linear momentum, and total angular momentum of the system.

Betsch et al. (2018) leveraged the tensor cross product, originally introduced by de Boer (1982) and reintroduced to the field of nonlinear continuum mechanics by Bonet et al. (2016). They subsequently adapted an EM scheme based on discrete gradients in the sense of Gonzalez (1996), to suit a mixed polyconvexity inspired elastodynamic framework. To achieve the desired multiphysics framework, we incorporate the mixed polyconvexity-inspired elastodynamics formulation by Betsch et al. (2018). This formulation is then extended by introducing additional fields from thermodynamics and electrostatics.

The paper is therefore organized as follows: In Section 2, fundamental concepts are presented, including the basics of the tensor cross products, a mixed Hu-Washizu-like variational potential for elastodynamics, balance equations derived from thermodynamics and electrostatics, and a suitable coupling energy density function. These elements collectively give rise to the mixed polyconvexity-inspired thermo-electro-mechanical framework. The temporal and spatial discretization is then discussed in Section 3. Using two examples, the structure-preserving properties of the formulation are investigated in Section 4, before brief conclusions are drawn in Section 5.

2. FRAMEWORK

In this section we give an overview of the balance equations of elastodynamics, thermodynamics and electrostatics along with a suitable material model yielding the fully coupled, mixed, polyconvexity-inspired framework we use.

2.1 Elastodynamics

We start with the elastodynamic part of the framework. The deformation gradient $\boldsymbol{F}$ defined as

$$\mathrm{d}\boldsymbol{x} = \boldsymbol{F}\ \mathrm{d}\boldsymbol{X} \tag{1}$$

10.1016/j.ifacol.2024.08.266

maps infinitesimal line elements $\mathrm{d}\boldsymbol{X} \in \mathcal{B}_0$ to their spatial counterparts $\mathrm{d}\boldsymbol{x} \in \mathcal{B}_t$, where $\mathcal{B}_0$ and $\mathcal{B}_t$ represent a body $\mathcal{B}$ in its reference and current configuration, respectively.

To describe the elastodynamic behaviour of the material under consideration we assume an energy density function of the form

$$\widehat{W}(\boldsymbol{C}) = \widetilde{W}(\boldsymbol{C}, \operatorname{cof}(\boldsymbol{C}), \det(\boldsymbol{C})) \tag{2}$$

with the right Cauchy Green tensor

$$\boldsymbol{C} = \boldsymbol{F}^{\mathrm{T}} \boldsymbol{F}. \tag{3}$$

We then utilize the tensor cross product [1] between two second-order tensors $\boldsymbol{A}, \boldsymbol{B} \in \mathbb{R}^3$ defined in index notation as

$$(\boldsymbol{A} \rtimes \boldsymbol{B})_{ij} = \epsilon_{i\alpha\beta}\, \epsilon_{jab}\, \boldsymbol{A}_{\alpha a}\, \boldsymbol{B}_{\beta b}, \tag{4}$$

where ϵ_{ijk} denotes the third-order permutation tensor. This operation allows us to rewrite the cofactor and the determinant of $\boldsymbol{C}$ as

$$\operatorname{cof}(\boldsymbol{C}) = \tfrac{1}{2}\,(\boldsymbol{C} \rtimes \boldsymbol{C}), \tag{5}$$

$$\det(\boldsymbol{C}) = \tfrac{1}{6}\,(\boldsymbol{C} \rtimes \boldsymbol{C}) : \boldsymbol{C}, \tag{6}$$

respectively. [2]

Note that the energy density function (2) can be viewed as objective version of the underlying polyconvex energy density function $\overline{W}(\boldsymbol{F}, \operatorname{cof}(\boldsymbol{F}), \det(\boldsymbol{F}))$.

We introduce the set of independent variables $\boldsymbol{\Sigma} = (\boldsymbol{C}, \boldsymbol{G}, C)$ for the right Cauchy Green tensor, its cofactor and its determinant along with the cascade like kinematic set

$$\begin{aligned} \boldsymbol{C} &= (\nabla\boldsymbol{\varphi})^{\mathrm{T}}\, \nabla\boldsymbol{\varphi}, \\ \boldsymbol{G} &= \tfrac{1}{2}\, \boldsymbol{C} \rtimes \boldsymbol{C}, \\ C &= \tfrac{1}{3}\, \boldsymbol{G} : \boldsymbol{C}. \end{aligned} \tag{7}$$

With a re-expressed energy density function

$$\widehat{W}(\boldsymbol{C}) = \bar{W}(\boldsymbol{C}, \boldsymbol{G}, C) \tag{8}$$

we can extend the classic variational potential for the pure displacement formulation by enforcing the kinematic set (7) via Lagrange multipliers $\boldsymbol{\Lambda} = (\boldsymbol{\Lambda}^{\mathbf{C}}, \boldsymbol{\Lambda}^{\mathbf{G}}, \Lambda^{C})$ yielding the 7-field Hu-Washizu type formulation

$$\begin{aligned} \Pi^{\mathrm{m}}(\boldsymbol{\varphi}, \boldsymbol{\Sigma}, \boldsymbol{\Lambda}) = \int_{\mathcal{B}_0} & \bar{W}(\boldsymbol{C}, \boldsymbol{G}, C) \\ & + \boldsymbol{\Lambda}^{\mathbf{C}} : \big((\nabla\boldsymbol{\varphi})^{\mathrm{T}}\, \nabla\boldsymbol{\varphi} - \boldsymbol{C}\big) \\ & + \boldsymbol{\Lambda}^{\mathbf{G}} : \big(\tfrac{1}{2}\, \boldsymbol{C} \rtimes \boldsymbol{C} - \boldsymbol{G}\big) \\ & + \Lambda^{C} : \big(\tfrac{1}{3}\, \boldsymbol{G} : \boldsymbol{C} - C\big)\ \mathrm{d}V + \Pi^{\mathrm{m,ext}}(\boldsymbol{\varphi}), \end{aligned} \tag{9}$$

where $\boldsymbol{\varphi}$ is the displacement field. A variation of (9) yields the seven stationary conditions

$$\begin{aligned} \delta_{\boldsymbol{\varphi}}\tilde{\Pi}^{\mathrm{m}} &= \int_{\mathcal{B}_0} \boldsymbol{\Lambda}^{\mathbf{C}} : \big((\nabla\delta\boldsymbol{\varphi})^{\mathrm{T}}\, \nabla\boldsymbol{\varphi} + (\nabla\boldsymbol{\varphi})^{\mathrm{T}}\, \nabla\delta\boldsymbol{\varphi}\big)\ \mathrm{d}V \\ &\quad + \Pi^{\mathrm{m,ext}}(\delta\boldsymbol{\varphi}) = 0, \\ \delta_{\mathbf{C}}\tilde{\Pi}^{\mathrm{m}} &= \int_{\mathcal{B}_0} \delta\boldsymbol{C} : \Big(\partial_{\mathbf{C}}\bar{W} - \boldsymbol{\Lambda}^{\mathbf{C}} \\ &\qquad + \boldsymbol{\Lambda}^{\mathbf{G}} \rtimes \boldsymbol{C} + \tfrac{1}{3}\, \Lambda^{C}\, \boldsymbol{G}\Big)\ \mathrm{d}V = 0, \\ \delta_{\mathbf{G}}\tilde{\Pi}^{\mathrm{m}} &= \int_{\mathcal{B}_0} \delta\boldsymbol{G} : \Big(\partial_{\mathbf{G}}\bar{W} - \boldsymbol{\Lambda}^{\mathbf{G}} + \tfrac{1}{3}\, \Lambda^{C}\, \boldsymbol{C}\Big)\ \mathrm{d}V = 0, \\ \delta_{C}\tilde{\Pi}^{\mathrm{m}} &= \int_{\mathcal{B}_0} \delta C \big(\partial_{C}\bar{W} - \Lambda^{C}\big)\ \mathrm{d}V = 0, \\ \delta_{\boldsymbol{\Lambda}^{\mathbf{C}}}\tilde{\Pi}^{\mathrm{m}} &= \int_{\mathcal{B}_0} \delta\boldsymbol{\Lambda}^{\mathbf{C}} : \big((\nabla\boldsymbol{\varphi})^{\mathrm{T}}\, \nabla\boldsymbol{\varphi} - \boldsymbol{C}\big)\ \mathrm{d}V = 0, \\ \delta_{\boldsymbol{\Lambda}^{\mathbf{G}}}\tilde{\Pi}^{\mathrm{m}} &= \int_{\mathcal{B}_0} \delta\boldsymbol{\Lambda}^{\mathbf{G}} : \big(\tfrac{1}{2}\boldsymbol{C} \rtimes \boldsymbol{C} - \boldsymbol{G}\big)\ \mathrm{d}V = 0, \\ \delta_{\Lambda^{C}}\tilde{\Pi}^{\mathrm{m}} &= \int_{\mathcal{B}_0} \delta\Lambda^{C}\ \big(\tfrac{1}{3}\, \boldsymbol{G} : \boldsymbol{C} - C\big)\ \mathrm{d}V = 0. \end{aligned} \tag{10}$$

Due to the arbitrariness of the variations we afterwards transform these equations into a set of differential equations to be able to augment our framework with the balance equations of the non-potential thermodynamic and the electrostatic field. We want to emphasize that the method shown here allows to augment the elastodynamic field with arbitrary not necessarily potential-based fields.

2.2 Thermodynamics and Electrostatics

For the thermodynamic extension we use the local energy balance

$$\theta\, \dot{\eta} = \bar{R} - \operatorname{Div} \boldsymbol{Q} \tag{11}$$

with the absolute temperature θ, the entropy density η, a prescribed heat source $\bar{R}$ and the Piola heat flux vector $\boldsymbol{Q}$. The formulation is completed by suitable thermal boundary and initial values.

For the electrostatic extension we take Maxwell's equations and neglect all transient and magnetic effects yielding Gauss's and Faraday's law

$$\begin{aligned} \operatorname{Div} \boldsymbol{D}_0 &= \bar{\rho}_0^{\mathrm{e}}, \\ \boldsymbol{E}_0 &= -\nabla\Phi \end{aligned} \tag{12}$$

with the electric potential Φ, the electric field $\boldsymbol{E}_0$, the electric displacement field $\boldsymbol{D}_0$ and a prescribed electric volume charge $\bar{\rho}_0^{\mathrm{e}}$. The formulation is completed by suitable boundary values for the electric potential and the electric surface charge. The present electrostatic formulation will later on result in a mixed finite element method in terms of Φ and $\boldsymbol{D}_0$, first presented by Ghandi and Hagood (1997).

2.3 Constitutive Equations

We extend the energy density function (8) to obtain a fully coupled thermo-electro-mechanical material model. For the numerical examples below we used the energy density function

$$\begin{aligned} W(\boldsymbol{C}, \boldsymbol{G}, C, \boldsymbol{D}_0, \theta) = & f_\theta(\theta)\, W_{\mathrm{em}}(\boldsymbol{C}, \boldsymbol{G}, C, \boldsymbol{D}_0) \\ & + W_{\mathrm{tm}}(C, \theta) + W_{\mathrm{t}}(\theta), \end{aligned} \tag{13}$$

where $W_{\mathrm{em}}(\boldsymbol{C}, \boldsymbol{G}, C, \boldsymbol{D}_0)$ is a compressible Mooney-Rivlin model with an ideal dielectric elastomer model. The full

[1] The tensor cross product was described in de Boer (1982) and later introduced to the field of nonlinear continuum mechanics by Bonet et al. (2016).

[2] For an overview on helpful properties and calculation rules for the tensor cross product cf. Betsch et al. (2018).

coupling of the model comes from the temperature dependent prefactor $f_\theta(\theta) = \frac{\theta}{\theta_\mathrm{R}}$. The thermomechanical and purely thermal contributions are given by

$$W_\mathrm{tm}(C,\theta) = -3\,\beta\,e\,(C-1)\,(\theta-\theta_\mathrm{R}), \tag{14}$$

$$W_\mathrm{t}(\theta) = \kappa\,\left(\theta - \theta_\mathrm{R} - \theta\,\log\left(\tfrac{\theta}{\theta_\mathrm{R}}\right)\right) \tag{15}$$

with the thermodynamical parameters β and e along with the reference temperature θ_R and the specific heat capacity κ. The given material model is convex with respect to $\{\boldsymbol{C}, \boldsymbol{G}, C, \boldsymbol{D}_0\}$ and concave with respect to θ. Note that while the energy density function's convexity is not mandatory, its presence not only enhances the stability of the formulation but also results in simpler equations when combined with the tensor cross product.

The description of the material model is completed by the constitutive equations of the three fields. The second Piola Kirchhoff stress tensor [3] denotes

$$\boldsymbol{S} = 2\left(\partial_{\mathbf{C}} W + \partial_{\mathbf{G}} W \barwedge \boldsymbol{C} + \partial_C W \boldsymbol{G}\right) \tag{16}$$

and the constitutive equations for the electrostatic and the thermodynamic fields are

$$\boldsymbol{E}_0 = \partial_{\mathbf{D}_0} W \quad , \quad \eta = -\partial_\theta W. \tag{17}$$

Finally, we use Fourier's law for thermal isotropy

$$\boldsymbol{Q} = -\boldsymbol{K}\nabla\theta \quad , \quad \boldsymbol{K} = k_0 C^{-1}\boldsymbol{G} \tag{18}$$

with the thermal conductivity coeffitient k_0 to conclude the material model.

2.4 Mixed Thermo-Electro-Mechanical Strong Form

We combine the mixed mechanical equations in strong form from Section 2.1 with the differential equations of thermodynamics (11) and elastostatics (12) which leads to the mixed strong formluation for thermo-electro-mechanics [4]

$$\begin{aligned}
\rho_0\,(\dot{\boldsymbol{\varphi}} - \boldsymbol{v}) &= \boldsymbol{0}\\
\mathrm{Div}(2\,\boldsymbol{F}\,\boldsymbol{\Lambda}^{\mathbf{C}}) + \bar{\boldsymbol{B}} &= \rho_0\,\dot{\boldsymbol{v}}\\
\theta\,\dot{\eta} + \mathrm{Div}\,\boldsymbol{Q} - \bar{R} &= 0\\
\mathrm{Div}\,\boldsymbol{D}_0 - \bar{\rho}_0^\mathrm{e} &= 0\\
\partial_{\mathbf{D}_0} W + \nabla\Phi &= \boldsymbol{0}\\
\partial_{\mathbf{C}} W - \boldsymbol{\Lambda}^{\mathbf{C}} + \boldsymbol{\Lambda}^{\mathbf{G}} \barwedge \boldsymbol{C} + \tfrac{1}{3}\,\Lambda^C\,\boldsymbol{G} &= \boldsymbol{0}\\
\partial_{\mathbf{G}} W - \boldsymbol{\Lambda}^{\mathbf{G}} + \tfrac{1}{3}\,\Lambda^C\,\boldsymbol{C} &= \boldsymbol{0}\\
\partial_C W - \Lambda^C &= 0\\
(\nabla\boldsymbol{\varphi})^\mathrm{T}\,\nabla\boldsymbol{\varphi} - \boldsymbol{C} &= \boldsymbol{0}\\
\tfrac{1}{2}\,\boldsymbol{C} \barwedge \boldsymbol{C} - \boldsymbol{G} &= \boldsymbol{0}\\
\tfrac{1}{3}\,\boldsymbol{G} : \boldsymbol{C} - C &= 0.
\end{aligned} \tag{19}$$

In order to arrive at the corresponding weak formulation, we multiply the equations from (19) with admissible test functions $\boldsymbol{w}_{(\bullet)}$, integrate over the entire body and apply integration by parts as usual.

[3] It is important to remark, that on a continuum level, (16) does not deviate from the well-known classical stress formula. However, the algorithmic form of the second Piola-Kirchhoff stress tensor will play a crucial role in preserving the energy conservation of the discrete system. The partial derivatives included are considerably simpler to calculate, due to the incorporation of both the polyconvex framework and the tensor cross product.

[4] The Lagrange multiplier $\boldsymbol{\Lambda}^{\mathbf{C}}$ can be understood as half of the second Piola-Kirchhoff stress tensor, i.e. $\boldsymbol{S} = 2\boldsymbol{\Lambda}^{\mathbf{C}}$.

3. DISCRETIZATION

In this section, we conduct the temporal and spatial discretization of the weak form outlined in Section 2.4 starting with the temporal one.

3.1 Structure Preserving Time Integration

For the temporal discretization we adopt the notion of discrete gradient introduced in Gonzalez (1996). Within this scheme the midpoint evaluations of the partial derivatives of W are substituted with discrete derivatives $\mathrm{D}_{\mathcal{V}} W$, which can be understood as algorithmic or time-discrete counterparts of $\partial_{\mathcal{V}} W$ with $\mathcal{V} \in \{\boldsymbol{C}, \boldsymbol{G}, C, \boldsymbol{D}_0, \theta\}$. These discrete derivatives fulfill the so called directionality condition

$$\begin{aligned}
W(\boldsymbol{\mathcal{V}}_{n+1}) - W(\boldsymbol{\mathcal{V}}_n) = \mathrm{D}_{\mathbf{C}} W : \Delta\boldsymbol{C}\\
+ \mathrm{D}_{\mathbf{G}} W : \Delta\boldsymbol{G} + \mathrm{D}_C W\,\Delta C\\
+ \mathrm{D}_{\mathbf{D}_0} W \cdot \Delta\boldsymbol{D}_0 + \mathrm{D}_\theta W\,\Delta\theta
\end{aligned} \tag{20}$$

with $\Delta(\bullet) = (\bullet)_{n+1} - (\bullet)_n$ thereby achieving the desired property of energy conservation - an aspect lacking in the classical midpoint evaluation. [5]

If we apply the time discretization including the discrete derivatives to the weak form, we obtain the semi-discrete set of equations

$$\begin{aligned}
&\int_{\mathcal{B}_0} \boldsymbol{w}_{\mathbf{v}} \cdot \left(\frac{1}{\Delta t}(\boldsymbol{\varphi}_{n+1} - \boldsymbol{\varphi}_n) - \boldsymbol{v}_{n+\frac{1}{2}}\right) \rho_0\,\mathrm{d}V = 0,\\
&\int_{\mathcal{B}_0} \boldsymbol{w}_{\boldsymbol{\varphi}} \cdot \frac{\rho_0}{\Delta t}(\boldsymbol{v}_{n+1} - \boldsymbol{v}_n)\\
&\quad + \boldsymbol{\Lambda}^{\mathbf{C}}_{n+1} : \left((\nabla\boldsymbol{w}_{\boldsymbol{\varphi}})^\mathrm{T}\,\nabla\boldsymbol{\varphi}_{n+\frac{1}{2}} + \left(\nabla\boldsymbol{\varphi}_{n+\frac{1}{2}}\right)^\mathrm{T}\nabla\boldsymbol{w}_{\boldsymbol{\varphi}}\right)\mathrm{d}V\\
&\quad + \Pi^{\mathrm{m,ext}}_{n+\frac{1}{2}}(\boldsymbol{w}_{\boldsymbol{\varphi}}) = 0,\\
&\int_{\mathcal{B}_0} w_\theta \left(\frac{1}{\Delta t}\,(\theta_{n+1}\eta_{n+1} + \theta_n\eta_n)\right.\\
&\qquad \left. - \frac{1}{\Delta t}(\theta_{n+1} - \theta_n)\mathrm{D}_\theta W\right)\,\mathrm{d}V\\
&\quad - \int_{\mathcal{B}_0} \nabla w_\theta \cdot \boldsymbol{Q}_{n+\frac{1}{2}}\,\mathrm{d}V + \Pi^{\mathrm{t,ext}}_{n+\frac{1}{2}}(w_\theta) = 0,\\
&\int_{\mathcal{B}_0} \nabla w_\Phi \cdot \boldsymbol{D}_{0_{n+\frac{1}{2}}}\,\mathrm{d}V + \Pi^{\mathrm{e,ext}}_{n+\frac{1}{2}}(w_\Phi) = 0,\\
&\int_{\mathcal{B}_0} \boldsymbol{w}_{\mathbf{D}_0} \cdot \left(\mathrm{D}_{\mathbf{D}_0} W + \nabla\Phi_{n+\frac{1}{2}}\right)\,\mathrm{d}V = 0\\
&\int_{\mathcal{B}_0} \boldsymbol{w}_{\mathbf{C}} : \left(\mathrm{D}_{\mathbf{C}} W - \boldsymbol{\Lambda}^{\mathbf{C}}_{n+1} + \boldsymbol{\Lambda}^{\mathbf{G}}_{n+1} \barwedge \boldsymbol{C}_{n+\frac{1}{2}}\right.\\
&\qquad \left. + \tfrac{1}{3}\Lambda^C_{n+1}\boldsymbol{G}_{n+\frac{1}{2}}\right)\,\mathrm{d}V = 0,\\
&\int_{\mathcal{B}_0} \boldsymbol{w}_{\mathbf{G}} : \left(\mathrm{D}_{\mathbf{G}} W - \boldsymbol{\Lambda}^{\mathbf{G}}_{n+1} + \tfrac{1}{3}\Lambda^C_{n+1}\boldsymbol{C}_{n+\frac{1}{2}}\right)\,\mathrm{d}V = 0,\\
&\int_{\mathcal{B}_0} w_C\left(\mathrm{D}_C W - \Lambda^C_{n+1}\right)\,\mathrm{d}V = 0\\
&\int_{\mathcal{B}_0} \boldsymbol{w}_{\boldsymbol{\Lambda}^{\mathbf{C}}} : \left(\left(\nabla\boldsymbol{\varphi}_{n+1}\right)^\mathrm{T}\nabla\boldsymbol{\varphi}_{n+1} - \boldsymbol{C}_{n+1}\right)\,\mathrm{d}V = 0,\\
&\int_{\mathcal{B}_0} \boldsymbol{w}_{\boldsymbol{\Lambda}^{\mathbf{G}}} : \left(\tfrac{1}{2}\boldsymbol{C}_{n+1} \barwedge \boldsymbol{C}_{n+1} - \boldsymbol{G}_{n+1}\right)\,\mathrm{d}V = 0,
\end{aligned} \tag{21}$$

[5] For the detailed construction rules of the discrete derivatives we refer to Franke et al. (2023).

$$\int_{\mathcal{B}_0} w_{\Lambda^C} \left(\tfrac{1}{3} \boldsymbol{G}_{n+1} : \boldsymbol{C}_{n+1} - C_{n+1} \right) \mathrm{d}V = 0.$$

where $f_{(\bullet)}$ denotes the evaluation of a variable f at time $t_{(\bullet)}$ along with $f_{n+\frac{1}{2}} = \frac{1}{2}(f_n + f_{n+1})$.

3.2 Finite Element Method

For the spatial discretization we employ the classic Bubnov-Galerkin finite element method along with the isoparametric concept. The continuous variables - namely, the displacement $\boldsymbol{\varphi}$, the temperature θ and the electric potential Φ - are approximated using 20-node serendipity shape functions. Regarding the mixed variables, which include the electric displacement vector $\boldsymbol{D}_0$ and the three mixed mechanical variables $\boldsymbol{C}$, $\boldsymbol{G}$ and C along with their corresponding Lagrange multipliers $\boldsymbol{\Lambda}^{\mathbf{C}}$, $\boldsymbol{\Lambda}^{\mathbf{G}}$ and Λ^C, we employ discontinuous trilinear Lagrange shape functions on eight-node cube elements. This enables the implementation of a static condensation, thereby reducing the numerical costs to approximately the level of a three-field thermo-electro-mechanical formulation.

4. NUMERICAL EXAMPLES

In this section we present two numerical examples showing the structure preserving properties of the formulation along with the possibilities in the field of boundary control.

4.1 Flying L-Shape

The first example is a technical one, where an L-shaped specimen can freely fly through space. Figure 1 shows the

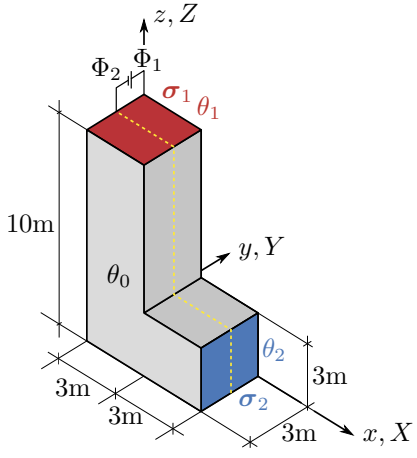

Fig. 1. Flying L-shape: reference configuration with boundary and initial conditions

specimens reference configuration along with its initial and boundary conditions. For the spatial discretization a total of 288 elements is used. The colored surfaces indicate initial temperatures of $\theta_1 = 250\mathrm{K}$ and $\theta_2 = 300\mathrm{K}$, whereas the remainder of the body starts with an initial temperature of $\theta_0 = 293.15\mathrm{K}$. For the first 5 seconds of the simulation, we apply mechanical Neumann boundary conditions in the form of two stresses

$$\boldsymbol{\sigma}_1(t) = -\boldsymbol{\sigma}_2(t) = f(t) \begin{pmatrix} 1 \\ 2 \\ 3 \end{pmatrix} \frac{\mathrm{N}}{\mathrm{m}^2} \tag{22}$$

with

$$f(t) = \begin{cases} \frac{256}{9} t & \text{for} \quad t \leq 2.5\mathrm{s} \\ \frac{256}{9}(5-t) & \text{for} \quad 2.5 \leq t \leq 5\mathrm{s} \\ 0 & \text{for} \quad t > 5\mathrm{s} \end{cases} \tag{23}$$

onto the two colored surfaces. Simultaneously, electrical Dirichlet boundary conditions corresponding to two electric potentials $\Phi_1(X, Y = 0, Z) = 0\mathrm{V}$ and $\Phi_2(X, Y = -1.5, Z) = 6 \cdot 10^6 \sin(\frac{\pi}{5} t)\mathrm{V}$ are applied on the back surface of the specimen and the surface indicated by the yellow dotted line (see Figure 1). The system is simulated over a total time $T = 40\mathrm{s}$ with a time step size $\Delta t = 0.8\mathrm{s}$. After the initial 5 seconds, as no additional energy is introduced into the system, the discrete gradient is able to preserve both the total energy E and the total angular momentum $||\boldsymbol{J}||$ as illustrated in Figures 2 and 3. Unlike the discrete gradient, the classic midpoint rule fails to preserve the total energy, resulting in an energy blow-up after a few seconds. Since the midpoint rule and the EM-scheme produce exactly the same results for the total angular momentum, only the EM-scheme is depicted in the bottom plots of Figures 2 and 3.

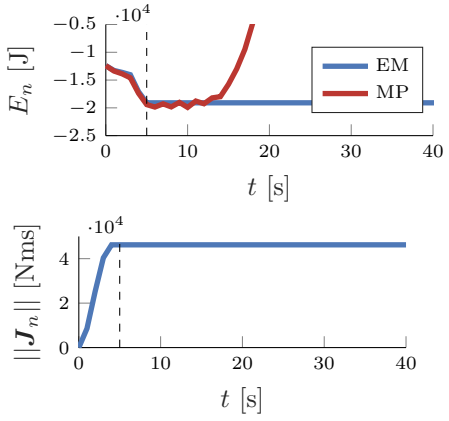

Fig. 2. Flying L-shape: total energy (top) and angular momentum (bottom)

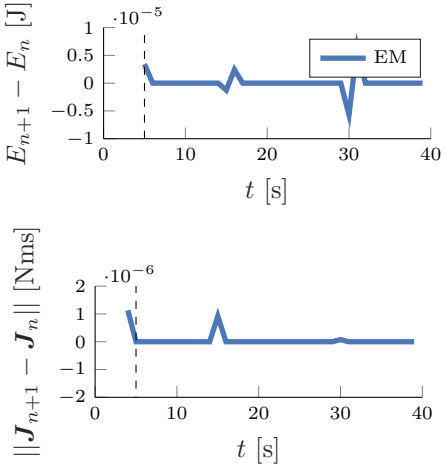

Fig. 3. Flying L-shape: difference of total energy (top) and angular momentum (bottom)

4.2 Microfluid Pumping Devise

As a second example, we illustrate a more practical application: a microfluid pump employed, for instance, to deliver drugs through the bloodstream. This example is intended to demonstrate both the long-term stability of the formulation and the possible applications in the area of boundary control. The microfluidic pumping device under consideration closely resembles the one discussed in e.g. Mehnert et al. (2017) and was also presented in Franke et al. (2023). Similarly, it does not account for fluid-structure interaction. Both the complete shape of the cylindrical pumping device and its dimensioning are depicted in Figures 4 and 5, where all lengths are provided in micrometers (μm). Due to the three symmetry axes, it is sufficient to simulate only one-eighth of the pumping corpus comprised of 320 finite elements, along with suitable symmetric mechanical Dirichlet boundary conditions. The simulation is conducted with a total simulation time of $T = 100$s and a time step size of $\Delta t = 0.1$s. The heating

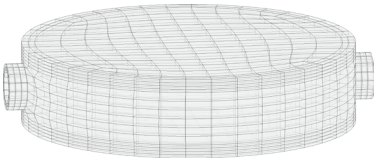

Fig. 4. Microfluid pump: initial configuration

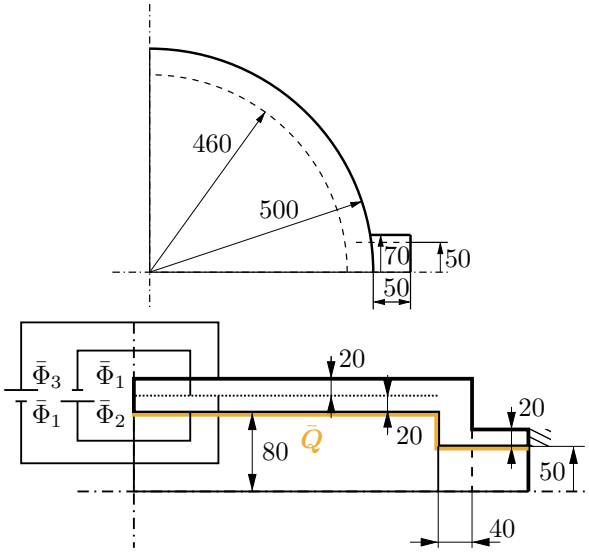

Fig. 5. Microfluid pump: top view (top) and side view (bottom) of one eighth of the pumping corpus

of the pumped liquid is simulated by a thermal Neumann boundary condition

$$\bar{Q} = 0.8 \begin{cases} t & \text{for } t \leq 2\,\text{s} \\ 4 - t & \text{for } 2\,\text{s} < t \leq 4\,\text{s} \\ 0 & \text{for } t > 4\,\text{s} \end{cases} \left[\frac{\text{W}}{\text{m}^2}\right], \tag{24}$$

applied to the interior of the pump for the initial 4 seconds of the simulation (illustrated in orange in Figure 5). For the pumping purpose two elastomer layers are sandwiched between two compliant electrodes on the top and bottom walls of the corpus, respectively. Specifically, mimicking the pumping movement involves applying Dirichlet boundary conditions in the form of electrical potentials $\bar{\Phi}_1$ to $\bar{\Phi}_3$, where $\bar{\Phi}_1 = 0$V at all times, while $\bar{\Phi}_2$ and $\bar{\Phi}_3$ follow a periodic pattern, as depicted in Figure 6. After the heating

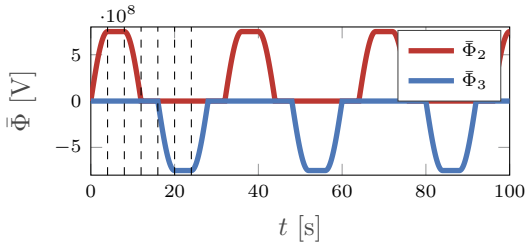

Fig. 6. Microfluid pump: periodically applied electric Dirichlet boundary conditions $\bar{\Phi}_2$ and $\bar{\Phi}_3$

phase and during constant phases of the applied electric potential fields the proposed EM integration scheme is able to correctly reproduce the conservation of the total energy of the system. Figure 7 shows the total energy and the energy difference [6] of the simulation with the proposed EM scheme. Finally, in Figure 8 snapshots of the simulation are

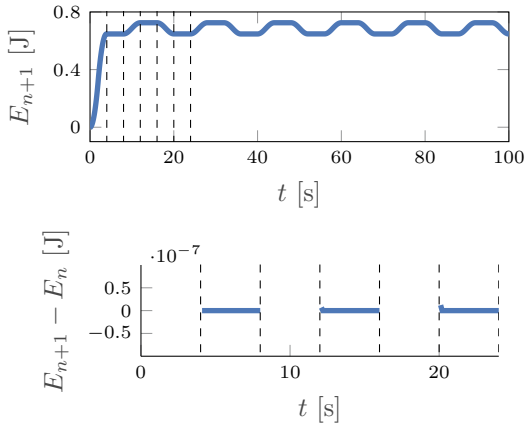

Fig. 7. Microfluid pump: total energy E (top) and total energy difference ΔE (bottom)

shown, where in column one to three the electric potential, the temperature and the von Mises stress are depicted. The top snapshot of each column takes place at time $t = 0$s, the middle one at time $t = 6$s and the bottom one shows each quantity at time $t = 22$s. The snapshots show that the formulation can accurately reproduce both the heating of the pump induced by the thermal Neumann boundary condition and the movement of the pump induced by the electrical Dirichlet boundary conditions.

5. CONCLUSIONS

This paper introduces a structure-preserving space-time discretization method for coupled nonlinear thermo-electro-elastodynamics. This approach is built upon the polyconvex mixed framework developed by Betsch et al. (2018), which has been further extended to accommodate multi-physics. To achieve this, the mixed Hu-Washizu-like seven-field variational potential was transformed into its corresponding strong form. Subsequently, it was augmented

[6] Note that the discrete energy difference is only plotted during time intervals when constant electric potential fields are applied.

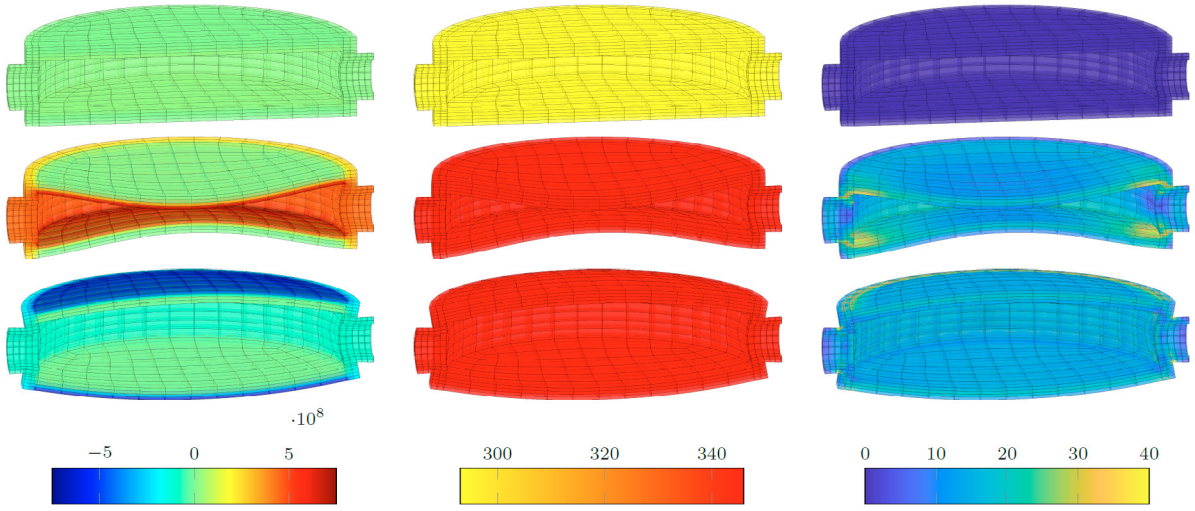

Fig. 8. Microfluid pump: snapshots of the electric potential field Φ [V] (left), the absolute temperature field θ [K] (center) and the von Mises stress σ_{vM} [Pa] (right) at times $t = 0$s (top), $t = 6$s (middle) and $t = 22$s (bottom).

with the requisite multiphysic fields, specifically incorporating thermodynamics and electrostatics in our case. In this augmentation, the selection of coupled fields is not confined solely to potential fields. The elastodynamic formulation's polyconvex structure derives advantages from the utilization of both the tensor cross product in conjunction with the cascade-like formulation of kinematic constraints and a polyconvex material model. The latter reflects the behavior of dielectric elastomers and is pivotal for the coupling within the formulation.

The result is a fully coupled mixed thermo-electro-elastodynamic framework, which was discretized in a next step using the finite element method and a structure-preserving time integration via discrete gradient in the sense of Gonzalez (1996) in space and time, respectively. Finally, two numerical examples were presented to demonstrate that the formulation exhibits numerical stability even in long-term simulations. Furthermore, the proposed method is capable to accurately preserve both the total energy and the total angular momentum of the system.

We see potential in transcribing the present formulation into the GENERIC formalism (see Öttinger (2005) and Schiebl and Betsch (2021)). GENERIC (General Equation for the Non-Equilibrium Reversible Irreversible Coupling) offers a thermodynamically consistent framework that splits the underlying evolution equations additively into reversible and irreversible parts. This aligns seamlessly with a possible extension of the formulation to incorporate viscoelastic material behavior, providing an even more accurate description of the behavior of dielectric elastomers.

REFERENCES

Betsch, P., Janz, A., and Hesch, C. (2018). A mixed variational framework for the design of energy-momentum schemes inspired by the structure of polyconvex stored energy functions. *Comput. Methods Appl. Mech. Eng.*, 335, 660–696. doi:10.1016/j.cma.2018.01.013.

Bonet, J., Gil, A.J., and Ortigosa, R. (2016). On a tensor cross product based formulation of large strain solid mechanics. *Int. J. Solids Structures*, 84, 49–63.

de Boer, R. (1982). *Vektor- und Tensorrechnung für Ingenieure*. Springer-Verlag Berlin Heidelberg.

Franke, M., Zähringer, F., Hille, M., Ortigosa, R., Betsch, P., and Gil, A. (2023). A novel mixed and energy-momentum consistent framework for coupled nonlinear thermo-electro-elastodynamics. *Int. J. Numer. Meth. Engng*, 124, 2135–2170. doi:10.1002/nme.7209.

Ghandi, K. and Hagood, N.W. (1997). Hybrid Finite Element Model for Phase Transitions in Nonlinear Electromechanically Coupled Material. In V.V. Varadan and J. Chandra (eds.), *Smart Structures and Materials 1997: Mathematics and Control in Smart Structures*, volume 3039, 97–112. International Society for Optics and Photonics, SPIE. doi:10.1117/12.276529.

Gonzalez, O. (1996). Time integration and discrete hamiltonian systems. *Journal of Nonlinear Science*, 6(5), 449–467. doi:10.1007/BF02440162.

Keplinger, C., Li, T., Baumgartner, R., Suo, Z., and Bauer, S. (2012). Harnessing snap-through instability in soft dielectrics to achieve giant voltage-triggered deformation. *Soft Matter*, 8, 285–288. doi:10.1039/C1SM06736B.

Mehnert, M., Hossain, M., and Steinmann, P. (2021). A complete thermo–electro–ciscoelastic characterization of dielectric elastomers, part i: Experimental investigations. *J Mech Phys Solids*, 157, 104603. doi:10.1016/j.jmps.2021.104603.

Mehnert, M., Pelteret, J.P., and Steinmann, P. (2017). Numerical modelling of nonlinear thermo-electro-elasticity. *Mathematics and Mechanics of Solids*, 22(11), 2196–2213. doi:10.1177/1081286517729867.

Öttinger, H. (2005). *Beyond Equilibrium Thermodynamics*. John Wiley & Sons.

Schiebl, M. and Betsch, P. (2021). Structure-preserving space-time discretization of large-strain thermo-viscoelasticity in the framework of GENERIC. *Int. J. Numer. Meth. Engng*, 122(14), 3448–3488. doi:10.1002/nme.6670.

Simo, J. and Tarnow, N. (1992). The discrete energy-momentum method. conserving algorithms for nonlinear elastodynamics. *Zeitschrift für angewandte Mathematik und Physik ZAMP*, 43, 757–792. doi:10.1007/BF00913408.